International Conference on Textile Composites and Inflatable Structures
STRUCTURAL MEMBRANES 2011
E. Oñate, B. Kröplin and K.-U.Bletzinger (Eds)

INVESTIGATION OF AN ELASTOFLEXIBLE MORPHING WING CONFIGURATION

BÉGUIN B.*, BREITSAMTER CH. * AND ADAMS N.*

*Institute of Aerodynamics and Fluid Mechanics
Technische Universität München
Boltzmannstr. 15, 85748 Garching, Germany
e-mail: benoit.beguin@aer,mw.tum.de, www.aer.mw.tum.de

Key words: Membrane wing, adaptive wing, experimental methods

Abstract. This paper considers the experimental investigation of a morphing wing using an elastic membrane for the lifting surface to allow large variations of the planform. Measurements of the membrane deflection of two different wing configurations at various flow conditions (i.e. dynamic pressure and angle of attack) are presented to provide insight into the complex flow-structure interaction mechanisms governing the behavior of the wing and help optimizing its aerodynamic performances. The results allow identifying the relative influence of the aerodynamic, geometric and structural parameters of the wing on the membrane deflection. In particular, the non-linearity of the interaction between the aerodynamic load and the membrane deflection is pointed out.

1 INTRODUCTION

1.1 Membranes in airplane design

In the history of airplane design, the use of thin, compliant membranes for the wing surfaces originates back to the beginnings of human flight. The wings of the "Wright Flyer" airplane, the world's first successful powered airplane developed by the Wright Brothers and flown in 1903, were made out of a thin membrane spanned over a rigid, load bearing structure [1]. Later, as aircraft had to fly faster and carry more payload, much stronger structures were required to withstand the aerodynamic loads acting on the airframe, discarding the use of membrane wings.

However, the low weight, low cost and structural simplicity of membrane wings still continued to make of them an attractive technical solution for low speed applications (typically hang glider, para glider). In the mid of the 20th century, membrane wings received attention with the development of the so called Princeton sailwing (Fig. 1a). It basically consists of a rigid leading edge spar and a trailing edge wire spanned between a tip rib and a root rib with a flexible membrane wrapped around the leading and trailing edges, forming the upper and lower wing

surfaces. Initially conceived as an advanced sail for a boat, it was later converted to an airplane wing. In Refs. [2] and [3], experimental tests of different sailwing configurations show that their aerodynamic characteristics compare favorably with conventional rigid wings in terms of maximum lift and maximum lift-to-drag ratio (i.e. aerodynamic efficiency). In particular, a notable feature of sailwings is their ability to naturally adapt their shape to changing flow condition, resulting superior stall characteristics.
More recently, membrane wings gained increased attention for their potential application in micro-sized aircraft design. The flow physics associated with the reduced size (similar to natural flyers) and low speed flight of these vehicles (i.e. low Reynolds number) differs passably from the behavior of conventional full scale aircrafts, and the use of flexible wing surfaces is found to be advantageous for this application. Investigations presented in Refs. [4] and [5] show that using a flexible wing surface facilitate shape adaptation, resulting in overall better performances.

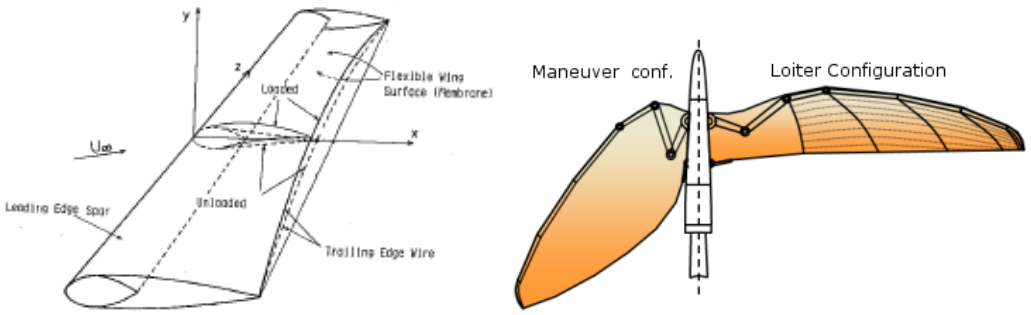

(a) (b)

Figure 1: a) Schematic structure of a Sailwing [6]. b) Sketch of the elastoflexible morphing wing: extension of the Princeton sailwing concept to a biologically inspired, form-variable wing.

1.2 The elastoflexible morphing wing

In recent years, an increased amount of resources is spent for the development of aircrafts able to considerably alter their shape with the goal to improve efficiency and expand flight envelope compared to conventional rigid configurations. In fact, the flight performances (efficiency and maneuverability) of an aircraft are directly related to its geometry and thus, in flight reconfiguration would allow a single aircraft to accomplish different mission roles efficiently and effectively ([7], [8]). A big challenge in the design of such morphing aircrafts lies in the contradictory requirements for the structure of high compliance to allow big deformations on the one hand, and structural integrity to withstand aerodynamic loads on the other hand.
In this context, this paper considers the investigation of a wing concept that uses the high compliance, low weight and adaptability advantages of membrane wings as a technical solution for such an extreme form-variable aircraft. The construction of this biologically inspired concept,

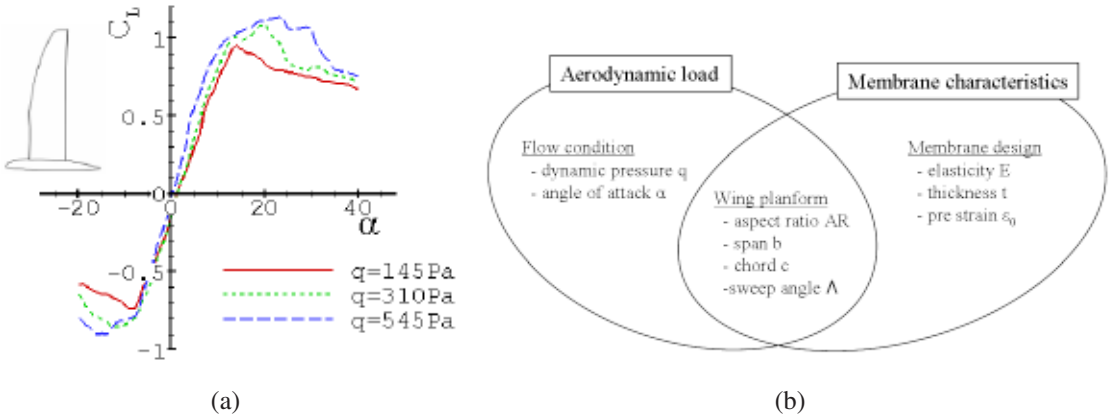

(a) (b)

Figure 2: a) Lift coefficient C_L as a function of the angle of attack α measured at different freestream dynamic pressures, illustrating the pronounced dependence of the aerodynamic characteristics on the flow conditions, [9]. b) Diagram showing the parameters involved in the aeromechanics of the elastoflexible morphing wing.

shown in Fig. 1b, basically consists of an articulating frame structure (leading and trailing edge spars) over which an elastic cover is spanned to form the aerodynamic surface. While the configuration of the leading edge spar, actively controlled, sets the overall planform of the wing, the highly extensible membrane used for the wing surface naturally adapts to the changing shape. Like this, a seamless aerodynamic surface can be obtained and the actuation can be done with reasonable actuation energy. With this particular design, the wing planform can be continuously varied between a high aspect ratio, straight wing and a highly swept back, low aspect ratio configuration (the so called "loiter" and "maneuver" configurations, respectively).
The investigation of this concept is carried out mainly experimentally by means of comprehensive tests of an appropriate wind tunnel model. So far, measurements of the lift, pitching moment and drag characteristics of several wing configurations allowed assessing the general behavior of the wing. The results (reported in Ref. [9]) show that overall, the active morphing of the wing planform effectively alters the lift and drag characteristics in such a way that a relatively high efficiency can be maintained over a wide range of flight conditions. However, due to its high compliance, the wing surface passively deforms under aerodynamic loading leading to a pronounced dependence of the aerodynamic characteristics on the flow conditions (see Fig. 2a). Thereby, the design of the membrane plays a determinant role.
In the present paper, the focus is set on quantitative measurements of the membrane deflection under various flow conditions, with the intention to better understand the behavior of the wing. The general trends are also compared with a simple model describing the aeromechanics of elastic sailwings.

1.3 Aeromechanics of sailwings

Due to its intrinsic construction, the shape of a membrane wing is not fixed in advance like for most common rigid wings. Rather, its shape results from the interaction between an aero-

dynamic flow field and a deformable surface. In Ref. [10], it is suggested that the maximum deflection of an elastic single-membrane wing is completely characterized by two parameters, the prestrain, ε_0, and a Weber number, We, expressing in this context the ratio of the aerodynamic load to the structural parameters of the membrane.

$$z_{max}/c = f(\varepsilon_0, We) \tag{1}$$

$$We = \frac{C_L q c}{E t} \tag{2}$$

where $q = \frac{1}{2}\rho U_\infty^2$ is the freestream dynamic pressure, c and t are the chord length and membrane thickness, respectively, and E the modulus of elasticity of the membrane[1]. C_L is the lift coefficient, expressing the fraction of the freestream dynamic pressure effectively converted into lift force, i.e., the actual aerodynamic load on the membrane. In Ref. [10], this model is found to match very well with experimental data. As far as a sailwing (i.e. double membrane) is considered in this paper and not a single membrane wing, additional considerations are necessary to extend the validity of Eq. (2). The main difference comes from the fact that, for a sailwing, the relative contribution of the upper and of the lower surfaces in the production of lift is different and therefore, the load acting on each surface is only a fraction of the whole C_L. As long as the upper and lower surfaces can be treated separately, Eq. (2) can be modified by a factor k_{up} and k_{low}, respectively, with $k_{low} = 1 - k_{up}$. Taking this into account, Eq. (2) results in

$$We_{up} = \frac{k_{up} C_L q c}{E t} \tag{3}$$

$$We_{low} = \frac{k_{low} C_L q c}{E t} = \frac{(1 - k_{up}) C_L q c}{E t} \tag{4}$$

Typically, the pressure load is less on the lower surface than on the upper one and a ratio of $k_{up} \approx 0.7$ and $k_{low} \approx 0.3$ can be assumed to be representative for positive angles of attack.
As shown in Fig 2b, in the case of the elastoflexible morphing wing considered here, the large planform variability increases the complexity of the interaction since a variation of the configuration simultaneously affects the membrane characteristics (via the prestrain) and the aerodynamic load. Beside the chord length c in the numerator of Eq. (2), the wing planform influences the aerodynamic loading via C_L, too. The influence of the planform on C_L can be taken into account using results of rigid wing theory ([1]) as follows. For angles of attacks in the attached flow regime, the lift coefficient C_L for a rigid wing is a linear function of the angle of attack α,

$$C_L = C_{L0} + C_{L,\alpha}\alpha \tag{5}$$

where C_{L0} is the lift coefficient at $\alpha = 0$. C_{L0} depends on the camber of the wing which, in the case of a membrane wing, is largely a function of the prestrain ε_0 ([6]). $C_{L,\alpha}$ is the slope of the lift curve, which directly depends on the planform of the wing via its aspect ratio (AR). Wings

[1] A linearly elastic material is assumed in this analysis.

with high aspect ratio (like the loiter configuration) provide a higher $C_{L,\alpha}$, thus produce more lift at equivalent flow conditions, than a low aspect ratio wing would do (like the maneuver configuration). Including Eq. (5) into Eq. (2) gives

$$z_{max,i}/c \quad \propto \quad \frac{k_i\left(C_{L0}+C_{L,\alpha}\alpha\right)qc}{Et} = \underbrace{\frac{k_i C_{L0} qc}{Et}}_{\propto 1/\varepsilon_0} + \underbrace{\frac{\left(k_i C_{L,\alpha}\alpha\right)qc}{Et}}_{\propto AR} \tag{6}$$

where i stands for either the upper or the lower surface. Eq. (6) models the aeromechanics of a sailwing taking into account the relevant aerodynamic, structural and geometric dependencies. The first term on the right hand side models the "initial" deflection at $\alpha = 0\ deg$ whereas the second term models how the deflection is expected to change with the angle of attack. The influence of the planform on the prestrain will be addressed in section 2.1.

2 EXPERIMENTAL TECHNIQUE

2.1 Wind tunnel model

The wind tunnel model used for the experimental investigations is shown in Fig. 3. An asymmetric cross section is used for the leading edge spar in order to provide better aerodynamic performances compared to a more simple rounded one. Table 1 gives a summary of the morphing capability of this model in terms of the relevant geometric parameters. The theoretical slope of the lift curve, $C_{L,\alpha}$, calculated for rigid wings of equivalent planforms and to be used in Eq. (6) are also given in this table 1[2].
The membrane currently used consists of an elastic fabric coated on one side with rubber layer[3] to ensure air impermeability. Table 2 gives an overview of the mechanical properties of this fabric as provided by the manufacturer (*Eschler Textile GmbH,*[12]). This material features anisotropic stiffness, and for its application in the wind tunnel model, the stiffer direction is aligned in chordwise direction. A suitable cut has been designed in order to avoid crinkles and provide the membrane with a certain pre-tension when mounted on the model even when the wing is in maneuver configuration. Obviously, due to the large planform variation, the pretension in the membrane depends on the configuration. Fig. 4 shows the prestrain of the membrane when mounted on the model for the loiter and maneuver configuration, measured on the lower side of the wing using a 2D photogrammetry technique. Here, the prestrain $\varepsilon_{0,\ chord}$ and $\varepsilon_{0,\ span}$ represent the elongation of the grid lines in the chordwise and spanwise directions, respectively, compared to the initial membrane cut. While the loiter configuration exhibits a much higher prestrain in spanwise direction due to its larger span (up to 40%) and almost no prestrain in the chordwise direction, the maneuver configuration exhibits just the opposite pattern with prestrain in chordwise direction up to 15%. Thereby, the prestrain in chordwise direction is supposed to have a greater influence on the deflection of the aerodynamically loaded membrane.

[2]Computed with a vortex lattice method ([11])

[3]Material composition as given by the manufacturer: 58% polyamide, 28% polyurethan, 14% spandex (Elastan).

(a) (b) (c)

Figure 3: Morphing wing model. a) articulating structure, b) Loiter configuration, c) Maneuver configuration

	Loiter conf.	Maneuver conf.	$\Delta_{Maneuver \rightarrow Loiter}$
Aspect Ratio AR [-]	8.6	4.6	$+87\%$
Sweep angle $\Lambda_{1/2}$ [^{o}]	6	36	-30^o
Area S [m^2]	0.23	0.2	$+15\%$
Half span $b/2$ [m]	1	0.6	$+67\%$
Mean chord c [m]	0.232	0.263	-12%
$C_{L,\alpha}$ (theoretical) [1/rad]	4.84	3.66	$+32\%$

Table 1: Geometric characteristics of the morphing wing model.

2.2 Test setup

The elastoflexible morphing wing model presented in Sec. 2.1 was tested in the low-speed wind tunnel facility "Windkanal A" of the Institute of Aerodynamics and Fluid Mechanics of the Technische Universität München. This wind tunnel has an open rectangular test section of 1.8 m height by 2.4 m width and 4.8 m length. It generates wind speeds up to 65 m/s with freestream turbulence below 0.4%.
The deflections of the upper and lower wing surfaces of the loiter and maneuver configurations have been measured at two wind speeds, namely $U_\infty = 15\ m/s$ and $30\ m/s$ ($q = 135\ Pa$ and

	Warp	Weft
Breaking load	$450\ N/5cm$	$290\ N/5cm$
Max. elongation	240 %	460 %
Modulus of elasticity (approx.)	$0.307\ MPa$	$0.616\ MPa$
Specific weight	$250\ g/m^2$	
Thickness	$0.5\ mm$	

Table 2: Overview of the mechanical properties of the membrane.

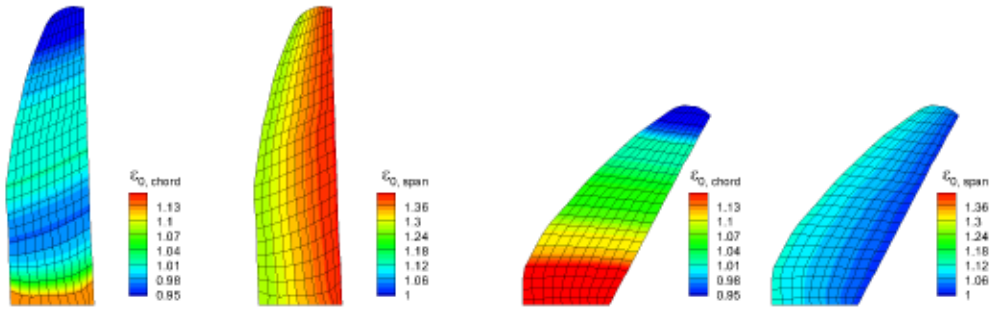

(a) Loiter configuration (b) Maneuver configuration

Figure 4: Prestrain for the membrane mounted on the model.

$q = 535\ Pa$) and for angles of attack of $\alpha = 0,\ 5,\ 10,\ 15$ and 20 deg[4]. The corresponding Reynolds numbers (based on the mean chord length) are $Re_{mac} = 0.232 \cdot 10^6$ and $0.464 \cdot 10^6$, resp., for the loiter configuration and $Re_{mac} = 0.263 \cdot 10^6$ and $0.526 \cdot 10^6$, resp., for the maneuver one.

2.3 Wing deflection measurements

The general setup for the deflection measurements is shown in Fig. 5. The stereo photogrametry system used is composed of two *FlowSense 2M* cameras placed outside of the wind tunnel test section with 40 deg angle of separation between the respective optical axes. The cameras have a resolution of 1600×1186 pixels which, in conjunction with the imaging optics (Nikon Nikkor, focal length 135 *mm*, aperture $1:28$) and the distance to the model, provides an average spatial resolution of 0.15 *mm* per pixel. A custom software using Direct Linear Transformation (*DLT*, [13]) technique is used to recover the 3D coordinates of markers put on each on the wing surface. A total of 230 markers (23 in spanwise and 10 in chordwise direction) consisting of white stickers of 5 *mm* diameter are used on each wing surfaces. A calibration target consisting of a 2D grid of markers defining the x-y plane and moved to several z-positions is used to obtain the transformation parameters necessary to reconstruct the coordinates in the object space with DLT. The reconstruction of the calibration points in the object space from the calibration images, using the transformation parameters obtained, indicates an average measurement uncertainty of 0.085 *mm* within the control volume. Finally, due to the small size of the control volume imposed by the imaging optics, the measurement of a whole wing consists of 11 single measurements patched together. For this, a traversing unit is used to move the measurement volume along the wing into the desired position. However, the traveling length of the traversing system used to measure the upper side is not sufficient to measure the complete wing in the loiter configuration. For this reason, results at the the wing tip for this side are not

[4]Results for the maneuver configuration at $\alpha = 20$ deg and $U_\infty = 30\ m/s$ could not be analyzed because of the strong vibration of the membrane.

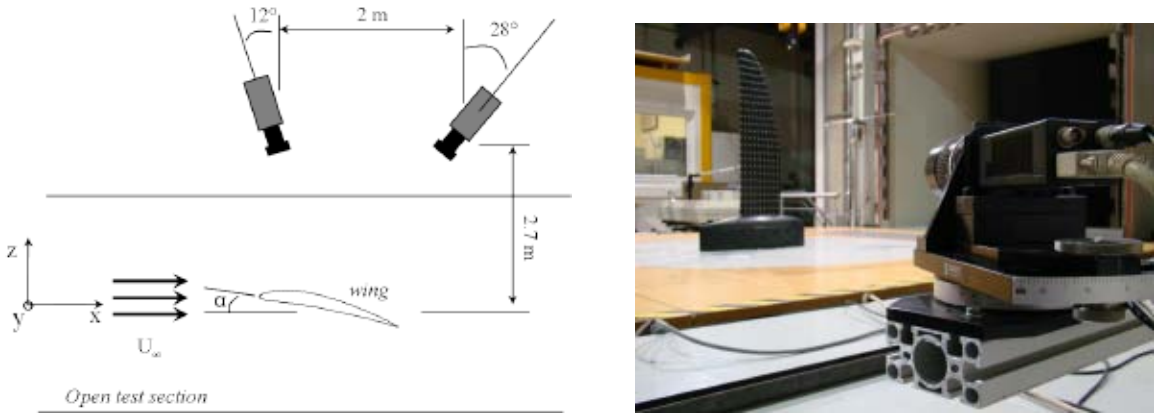

(a) (b)

Figure 5: a) Schematic of the experimental setup (measurement of the wing upper side, similar setup used to measure the lower side). b) Real setup.

available.

3 RESULTS AND DISCUSSION

3.1 Membrane deflection

To show the overall deformation pattern, Fig. 6 presents the normal membrane deflection Δz measured for the case $q = 535\ Pa$ and $\alpha = 5\,\text{deg}$. Due to the airflow accelerating over the wing upper side, a lower pressure occurs there that creates a suction force, thus the upward deflection of the membrane (positive z-direction). On the lower side, the pressure increases and the membrane deflects in the same direction than for the upper side but with lower amplitude since the pressure load is less on this side. In the case of the loiter configuration, the influence of the inner wing structure (cf. Fig. 3a) is visible on the lower left part. The membrane comes in contact with the linkages, limiting the deflection in this region. Regarding the deflection pattern, both configurations exhibit a maximum deflection in the inner part of the wing with a "zero" deflection on the boundary since the membrane is there constrained by the frame structure. Similar deformation patterns were observed in the other cases.

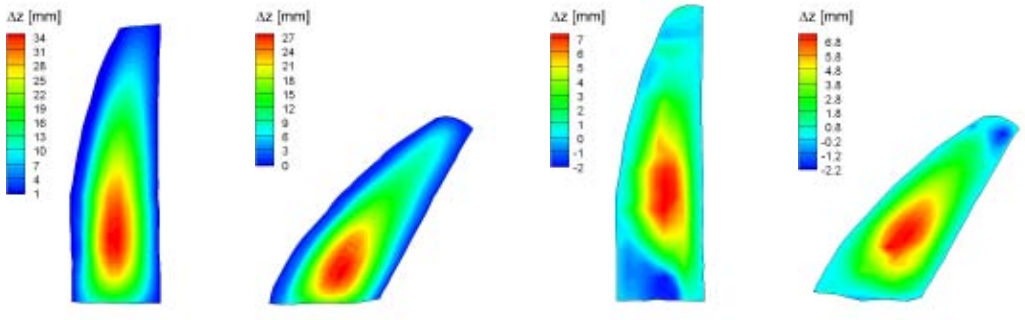

(a) Upper side (b) Lower side

Figure 6: Normal deflection of the membrane (Δz) at $q = 535\ Pa$ and $\alpha = 5\ deg$.

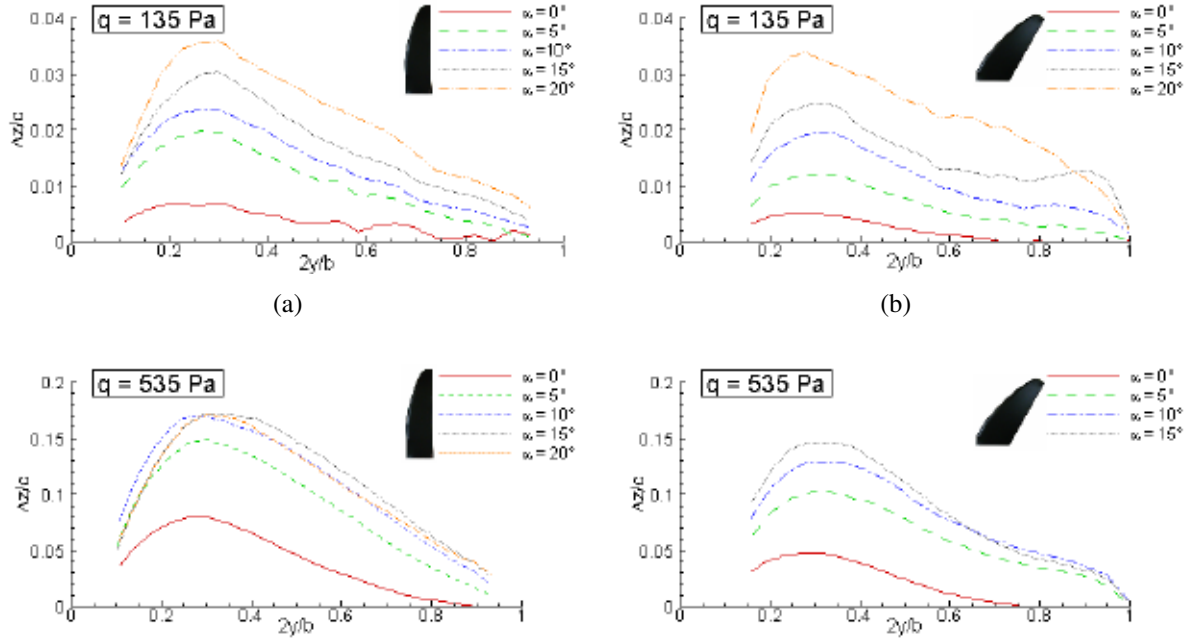

(a) (b)

(c) (d)

Figure 7: Spanwise distribution of the maximum deflection of the upper side.

Fig. 7 shows the spanwise distribution of the deflection $\Delta z/c$ (i.e. maximum deflection in each spanwise section) of the upper side of the loiter and maneuver configurations as a function of the angle of attack for both dynamic pressures investigated. In all cases, similar shapes are found with a "zero" deflection at the root as well as at the tip because the membrane is fixed on the structure there. Generally, the camber (i.e. deflection) grows roughly monotonically with the angle of attack. In all cases, except the one in Fig. 7b, the deflection grows more rapidly between $\alpha = 0$ deg and $\alpha = 5$ deg than for higher angles of attack. This so called hysteresis effect

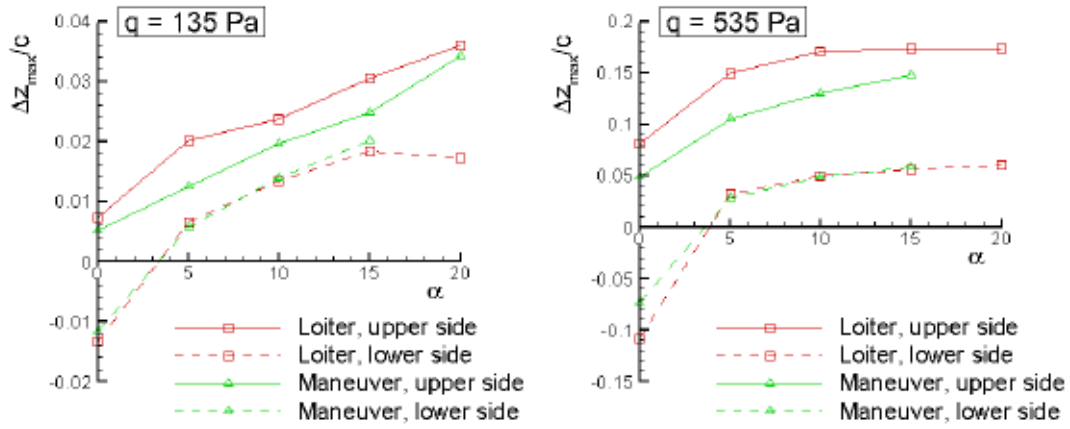

(a) $q = 135\ Pa$ (b) $q = 535\ Pa$

Figure 8: Evolution of the maximum deflection $\Delta z_{max}/c$ with the angle of attack α.

occurs because the situation around $\alpha = 0$ deg is unstable since the direction of the aerodynamic load is not clearly defined. At higher angles of attack, however, the direction is uniquely defined and the membrane "snaps" to a stable shape. This effect is known to be strongly dependent on the pretension of the membrane, which is also verified here since it is more pronounced in the case of the loiter configuration where the chordwise prestrain is much lower than for the maneuver configuration (see Fig. 4). Fig. 7c exhibits some additional features. The deflection increases only between $\alpha = 0\ deg$ and $\alpha = 10\ deg$ but not further. This may be explained twofold. On the one hand, the onset of stall as a result of the high camber and relative high angle of attack limits the aerodynamic load, discarding a further increase of the deflection. On the other hand, due to the high deflection, the membrane has reached an elongation from which its stiffness increases, making a further increase of the deflection impossible. Finally, comparing the respective shape of the deflection along the span, the loiter and maneuver configuration show some clearly different characteristics. In the maneuver configuration, the decrease of the deflection after the maximum towards wing tip is steeper but the camber overall higher at the tip than for the loiter configuration. This is supposedly due to the difference in spanwise pretension between both configurations.

3.2 Comparison of the maximum deflection with the theoretical model

Fig. 8 shows the evolution of the maximum deflection with the angle of attack of the upper and lower wing surfaces. The characteristics observed in the previous section concerning the upper side can be generalized to the lower surface. In particular, the rapid increase in $\Delta z_{max}/c$ between $\alpha = 0\ deg$ and $\alpha = 5\ deg$, characteristic of the hysteresis effect, can be well observed. In the following, the principal trends observed in Fig. 8 are compared to the predictions of the theoretical model presented in Sec. 1.3.

First of all, Eq. (6) predicts that the maximum deflection scales with the dynamic pressure. This can be well observed here since the amplitude of $\Delta z_{max}/c$ at $q = 535\ Pa$ is much higher than the deflections measured at $q = 135\ Pa$. However, the dependency is not linear since the lift coefficient C_L, which also plays a role in Eq. 6, also depends on q in the case of a sailwing (see Fig. 2). Here, the non-linearity of the aeromechanics of a sailwing becomes clear: a higher dynamic pressure induces a higher deflection, which in turn increases the aerodynamic load until an equilbrium is reached. The simple linear relation for C_L considered in section 1.3, Eq. 5, is not sufficient to completely describe the behavior of a sailwing and a more complex relation in the form of $C_L = f(\alpha,\ q,\ \varepsilon_0)$ should be used.
The deflection in the case of the maneuver configuration is overall lower than for the loiter one (at least for the upper side), which confirms the dependency between the prestrain and the deflection amplitude assumed in Sec. 1.3, namely that a higher prestrain limits the deflection. Surprisingly however, the deflections of the lower surfaces of both configurations are very similar, which may be explained by the presence of the linkages of the inner wing structure, as mentioned in Sec. 3.1.
From Eq. 6, the planform is supposed to influence the rate of growth of the deflection with the angle of attack, via $C_{L,\alpha}$ and c. Looking at the respective values of these two parameters for both configurations in Tab. 1, the lower $C_{L,\alpha}$ of the maneuver configuration is somehow compensated by its higher chord but overall, a slightly lower rate would be expected. In Fig. 8, the curves of both configurations feature very similar slopes and the hysteresis effect makes it difficult to discern a clear trend.
Finally, as a result of the different pressure load on the upper and lower wing surfaces, the model of Sec. 1.3 predicts lower deflections of the lower than of the upper surface. This trend can be fairly observed in Fig. 8.

4 CONCLUSION AND OUTLOOK

This paper considers the experimental investigation of a morphing wing using an elastic membrane for the lifting surface to allow large variations of the planform. Measurements of the membrane deflection of two different wing configurations at various flow conditions (dynamic pressure and angle of attack) were performed to investigate in more details the complex flow-structure interaction mechanisms governing the behavior of the wing. For this, a stereo photogrammetry system using the Direct Linear Transformation method is used. Also, a simple theoretical model describing the aeromechanics of elastic sailwings taking into account the principal geometric, structural and aerodynamic dependencies is also presented.
Measurement results highlights the strong dependency of the membrane shape on the flow conditions, which is responsible for the unconventional aerodynamic characteristics of the wing. The influence of the planform variability on the deflection of the membrane is pointed out and thereby, the major influence comes from the varying prestrain associated with the different configurations. The pure influence of the planform on the aerodynamic load can not be clearly identified in this case. Finally, the results highlights the strong non-linear dependency between the aerodynamic load and the membrane deflection, indicating a limited validity of the basic

aeromechanic model.
Taking advantages of these results, further work will consider new membrane design with the main goal to optimize the aerodynamic performances of the wing. For this, not only wind tunnel tests but also numerical simulations are planned.

REFERENCES

[1] J. D. Anderson. *Aircraft Performances and Design*. McGraw-Hill International Editions, 1996.

[2] M. P. Fink. Full-scale Investigation of the Aerodynamic Characteristics of a Sailwing of Aspect Ratio 5.9. Technical report, NASA, Langley Research Center, 1969.

[3] M.D. Maughmer. A Comparison of the Aerodynamic Characteristics of Eight Sailwing Airfoils Sections. Technical report, Princeton Unversity.

[4] Yongsheng L. and Shyy W. Laminar-Turbulent Transition of a Low Reynolds Number Rigid or Flexible Airfoil. *AIAA Journal*, 45:pp. 1501–1513, 2007.

[5] Hu H. and Tamai. Flexible-Membrane Airfoils at Low Reynolds Number. *Journal of Aircraft*, 45:pp. 1767–1778, 1099.

[6] H. Murai and S. Maruyama. Theoretical Investigation of Sailwing Airfoils Taking Account of Elasticities. *Journal of Aircraft*, 19(5):pp. 385–389, 1982.

[7] M. Abdulrahim and R. Lind. Using Avian Morphology to Enhance Aircraft Maneuverability. In *AIAA Atmospheric Flight Mechanics Conference and Exhibit*, August 2006.

[8] A.R. Rodriguez. Morphing Aircraft Technology Survey. In *45th AIAA Aerospace Sciences Meeting and Exhibit*, January 2007.

[9] B. Beguin and C. Breitsamter. Experimental Investigations of an Elasto-flexible Morphing Wing Concept. In *27th International Congress of the Aeronautical Sciences*, number ICAS-2010-2.10.4, September 2010.

[10] Song A. and Tian X. Aeromechanics of membrane wings with implications for animal flight. *AIAA Journal*, 46(8), 2008.

[11] M. Drela and H. Youngren. AVL - Aerodynamic Analysis, Trim Calculation, Dynamic Stability Analysis, Aircraft Configuration Developpement. http://raphael.mit.edu/avl. v.3.15.

[12] Eschler Textil GmbH. http://www.eschler.com.

[13] Luhmann T. *Close Range Photogrammetry*. Wiley, 2nd edition, 2006.